Academic Journal of Emerging Technologies
ISSN Print: 3104-4417
ISSN Online: 3104-4425
CD ISSN: 3104-4433
https://doi.org/10.63313/AJET.9011

Superhydrophobic HWCNTs/EP composite coating with anti-icing and photothermal deicing properties

Haiyang Zhang. Youqiang Wang* and Guijing Guo
School of Mechanical and Automotive Engineering, Qingdao University of Technology, Qingdao 266520, China
Email: zhy994845257@163.com

How to cite this paper: Zhang, H., Wang, Y., & Guo, G. (2025). Superhydrophobic HWCNTs/EP composite coating with anti-icing and photothermal deicing properties. Academic Journal of Emerging Technologies, 1(2), 48-65. ISSN Print: 3104-4417; ISSN Online: 3104-4425.
https://doi.org/10.63313/AJET.9011
Published: 2025-10-16

Abstract

Photothermal superhydrophobic surfaces have garnered significant attention for their exceptional anti-icing and photothermal deicing capabilities. However, the shortcomings of stability and fabrication complexity limit their practical application. This work designed and fabricated a HWCNTs/EP composite coating that combines anti-icing/deicing performance, and facile preparation. During fabrication, the HWCNTs and EP ratio was systematically optimized by evaluating wettability, photothermal conversion capability, and anti-icing/deicing performance. The composite coating in the ratio of HWCNTs/EP 1:1 exhibited a water CA of 156.7°. Photothermal testing revealed a maximum temperature increase of 69 ℃ (reached in 200 s) under one sun intensity. The composite coating demonstrated a prolonged droplet freezing time of 1026 s at −15 ℃. Photothermal deicing testing achieved complete ice melting and detachment within 44 s. This work provides novel insights for designing stable photothermal superhydrophobic coatings with anti-icing/deicing functionality, contributing to the development of energy-efficient ice mitigation technologies.

Keywords

Superhydrophobicity; Photothermal deicing; Anti-icing; Photothermal conversion

1. Introduction

In low-temperature conditions, icing phenomena significantly impact daily life and pose potential safety risks in industrial operations[1]. In power transmission systems, ice accretion on cables may damage or fracture transmission lines, potentially triggering large scale power outages[2]. In aviation and maritime sectors, ice formation on aircraft wings or ship propellers increases weight, reduces operational speed, and may compromise structural integrity[3-5]. While conventional deicing methods—including mechanical removal[6], chemical deicers[7], and electrothermal deicing[8]can effectively eliminate ice layers to some extent, they frequently

suffer from limitations such as relatively low efficiency, high operational costs, and potential environmental impacts[9]. Consequently, developing stable and sustainable anti-icing/deicing coatings remains critical.

Superhydrophobic surfaces, characterized by extremely high water contact angles and low rolling angles, prevent water droplet wetting by inducing droplet rebound or rolling off[10]. This unique property grants them promising potential in passive anti-icing applications. For example，the novel superhydrophobic surface fabricated on aluminum conductors through a two-step anodization technique[11] and the calcium sulfate whisker-reinforced thermoplastic polyurethane composite coating[12] both demonstrate significant enhancements in surface ice accumulation resistance and freezing delay capabilities. Nevertheless, surface icing remains inevitable under low-temperature/high-humidity conditions. As a green and clean energy source, sunlight inherently exhibits ice-melting capabilities. Based on this, researchers have focused on harnessing solar energy. While solar energy has been well-established in photovoltaic power generation[13], photobiological utilization[14], and photochemical applications[15], its application in photothermal deicing[16] remains relatively underdeveloped. Consequently, researchers have developed photothermal superhydrophobic surfaces with active deicing functionality by incorporating photothermal fillers such as carbon powder[17, 18], carbon nanotubes[19-21], titanium nitride[22], graphene[23-25], and polydopamine[26-28], combined with hydrophobic nanoparticles. These surfaces efficiently melt ice through solar-to-thermal energy conversion, facilitating rapid residue-free ice removal and transforming deicing technologies. The design strategy for such surfaces involves two synergistic approaches: 1) enhancing anti-icing performance through microstructure optimization based on wettability theory, and 2) improving photothermal deicing efficiency in low-temperature environments by leveraging photothermal materials[29-31]. This dual mechanism provides critical insights for developing highly efficient and eco-friendly anti-icing/deicing surfaces. Photothermal superhydrophobic surfaces not only prevent ice formation by repelling water droplets but also actively remove pre-existing ice through localized heating[32]. Compared to conventional superhydrophobic surfaces, they integrate anti-icing and photothermal deicing capabilities, positioning them as highly promising solutions for ice prevention/removal applications. The technological advantages have been validated through multiple innovative fabrication processes: Gou et al.[33] implemented a modified SiO2/graphene nanocomposite coating on copper substrates via spraying technology, which extended droplet freezing time by fivefold and enhanced photothermal deicing efficiency by 90%. Li et al.[34] employed multi-pulse laser sintering combined with HDTMS chemical modification on carbon steel surfaces, achieving fourfold prolongation of droplet freezing duration and complete ice melting under 210-second intensity. Liu et al.[35] developed a TiO2/MWCNTs composite epoxy coating exhibiting tenfold ice formation delay and rapid photothermal deicing

within 20 seconds. However, durability and stability remain persistent challenges for superhydrophobic coatings. Practical large-scale deployment further requires addressing critical prerequisites such as scalable manufacturing and cost-effectiveness, posing significant design challenges for photothermal superhydrophobic coatings[36-38]. A representative design strategy involves embedding photothermal fillers into resin matrices. Resins can enhance coating durability and stability through their mechanical robustness, strong adhesion, and chemical resistance. Nevertheless, achieving superhydrophobicity typically necessitates surface modification of photothermal fillers, complicating fabrication processes. Consequently, low-surface-energy substrates like silicone-fluorocarbon resins[39] and silicone resins[40] have become preferred matrices for photothermal superhydrophobic coatings.

In this work, a HWCNTs/EP composite coating with anti-icing/deicing performance was designed and prepared by combining the epoxy resin and HWCNTs. The successful incorporation of low-surface-energy functional groups into epoxy resin via chemical grafting endows the coating with enhanced hydrophobicity and stability. This methodology offers advantages of simplified processing and cost-effectiveness for scalable fabrication. The HWCNTs establishes a nano structure that confers superior superhydrophobicity and effective photothermal conversion capability, while the epoxy resin binder ensures robust interfacial adhesion to substrates and enhanced wear resistance. Results confirm that the fabricated coating retains both superhydrophobic properties and photothermal performance following rigorous durability testing. This work provides critical insights for designing durable photothermal superhydrophobic surfaces for anti-icing applications, facilitating the practical implementation of photothermal superhydrophobic technologies.

2. Experimental

2.1. Materials

The experimental materials were as follows: AZ31B magnesium alloy plates were purchased from Dongguan Hongdi Metal Materials Co., Ltd. Bisphenol A-based epoxy resin (E51) and curing agent (D230) were obtained from Nanchang Chenfang Adhesive Products Co., Ltd. Hydroxylated multi-walled carbon nanotubes (HWCNTs, 95% purity, with an outer diameter of 20 nm) were acquired from Sinopharm Chemical Reagent Co., Ltd. Silane coupling agent (KH550) was purchased from Aladdin Biochemical Technologies Co., Ltd. 1H,1H,2H,2H-perfluorodecyltrimethoxysilane (FAS) was obtained from Shanghai Macklin Biochemical Co., Ltd. Pellet-shaped sodium hydroxide, anhydrous ethanol (99.7%), and ethyl acetate were supplied by Tianjin Fuyu Fine Chemical Co., Ltd. All reagents were of analytical grade and used without further purification.

2.2. Preparation of HWCNTs/EP Photothermal Superhydrophobic

Coating

Magnesium alloy plates (20 mm × 20 mm × 1 mm) were mechanically polished with 800, 1200, and 2000 grit sandpapers to remove surface oxides, followed by ultrasonic cleaning in anhydrous ethanol for 10 minutes. The cleaned substrates were dried with a cold air blower and stored for subsequent use. The synthesis of the HWCNTs/EP photothermal superhydrophobic coating is schematically illustrated in Fig.1. First, a mixture of 1 g KH-550 and 0.2 mL NaOH (0.25 mol/L) solution was prepared in 10 mL anhydrous ethanol. The solution was stirred at 60°C for 2 hours to ensure complete hydrolysis of KH-550. Subsequently, 0.5 g FAS was added to the reaction mixture, and the stirring was continued for an additional 2 hours to obtain a transparent fluorinated oligomer. To prepare the modified epoxy resin (EP-M), the synthesized fluorinated oligomer was mixed with epoxy resin at a mass ratio of 5:1 and dispersed in 10 mL ethyl acetate under magnetic stirring for 30 minutes. Next, different mass ratios of EP and HWCNTs were dispersed in 10 mL ethyl acetate under magnetic stirring for 30 minutes. The specific mass ratios of EP and HWCNTs are listed in Tab.1. After adding 0.2 g D230 as a curing agent, the mixture was stirred for an additional 10 minutes to form a homogeneous solution. The coating solution was sprayed onto the pre-treated magnesium alloy substrate and cured at 80°C for 3 hours to obtain the final photothermal superhydrophobic coating

Tab 1. the mass ratio of EP/HWCNTs

HWCNTs	0.2g	0.2g	0.2g	0.2g	0.2g
EP	0g	0.2g	0.4g	0.6g	0.8g

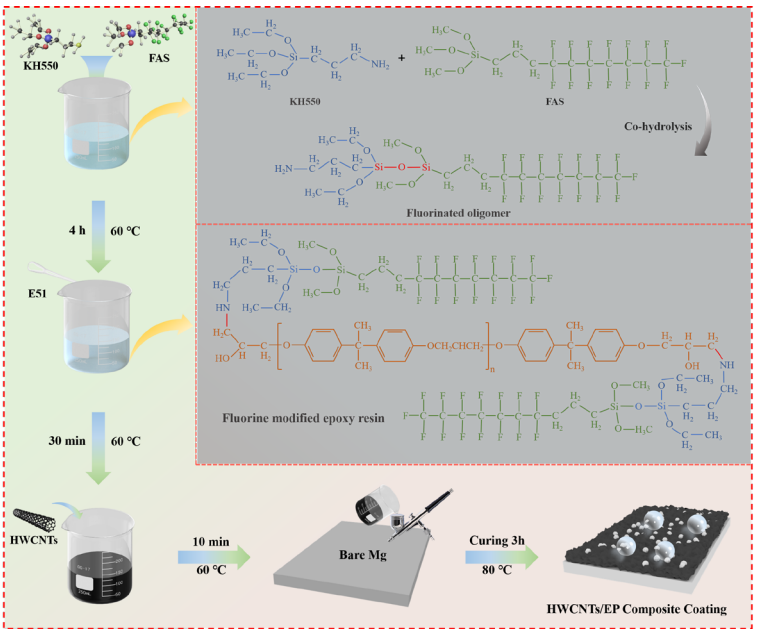

Fig 1. Preparation of HWCNTs/EP composite coating.

3. Results and discussion

3.1. Surface morphology and chemical composition

Fig. 2 presents the surface microstructures and corresponding structural characterization of HWCNTs/EP composite coatings with different ratios. When the EP mass was 0g, the SHC0/4 coating exhibited a uniformly distributed porous microstructure (Fig. 2a). EDS analysis revealed homogeneous elemental distribution on the surface, predominantly composed of C (72.2%), O (18.2%), and F (5%), with trace amounts of Si derived from KH550 and FAS (Fig. 2b). The three-dimensional laser confocal microscopy topography demonstrated a surface roughness of 4.5 μm for the coating (Fig. 2c). When the EP mass adjusted to 0.2g (Fig. 2d), the SHC1/3 coating displayed pronounced larger spherical aggregates with nano-mastoid structures on the surface and abundant voids, formed by the agglomeration and stacking of HWCNTs on EP surfaces. Compared to the SHC0/4 coating, the C content decreased while the Si content increased due to the addition of EP. The formation of these spherical structures resulted in an elevated surface roughness of 6.4 μm (Fig. 2e-f). As evidenced in Fig. 2g-i, when the addition amounts of EP was 0.4g, the SHC1/1 coating exhibited a substantial increase in spherical aggregates on its surface, accompanied by a denser distribution of nano-mastoid structures. A noticeable reduction in surface voids was observed, resulting in enhanced coating compactness. Notably, the surface roughness reached a maximum value of 15.4 μm under these conditions. As illustrated in Fig. 2j, the SHC3/1 coating demonstrates predominant spherical surface structures with increasing EP proportion, though accompanied by a marked reduction in nano-mastoid structures. This phenomenon is ascribed to diminished surface aggregation of EP caused by the decreased HWCNTs ratio. When exclusively incorporating EP, the SHC4/0 coating exhibits further increased spherical structures and enhanced surface smoothness, with nano-mastoid being virtually absent (Fig. 2m). EDS elemental mapping reveals significant compositional alterations: C content decreases to 37.3% while Si content rises to 23%, concurrent with reduced surface roughness to 5.5 μm (Fig. 2n-o). The synergistic interplay between EP and HWCNTs establishes a hierarchical micro-nano architecture that fundamentally enables the coating's superhydrophobic surface characteristics.

As revealed by Fourier transform infrared (FTIR) spectroscopy analysis of coating samples (Fig. 3), both EP and EP-M exhibit characteristic absorption bands at 2928 cm^{-1} and 2868 cm^{-1}, corresponding to the stretching vibrations of methyl ($-CH_3$) and methylene ($-CH_2$) groups in the epoxy resin[41]. The intensified peak intensities observed in EP-M originate from increased methyl/methylene groups through KH550 and FAS grafting. Absorption peaks at 1616 cm^{-1} and 1509 cm^{-1} are attributed to aromatic ring stretching vibrations in the epoxy matrix[37]. Notably, compared with pristine EP, EP-M demonstrates two new characteristic peaks at 1096 cm^{-1} and 1211 cm^{-1}, assigned to asymmetric Si-O-Si stretching and C-F bond

vibrations respectively[42]. These emerging peaks confirm the successful grafting of KH550 and FAS, effectively introducing low surface energy functional groups into the epoxy resin, thereby verifying the successful chemical modification of EP.

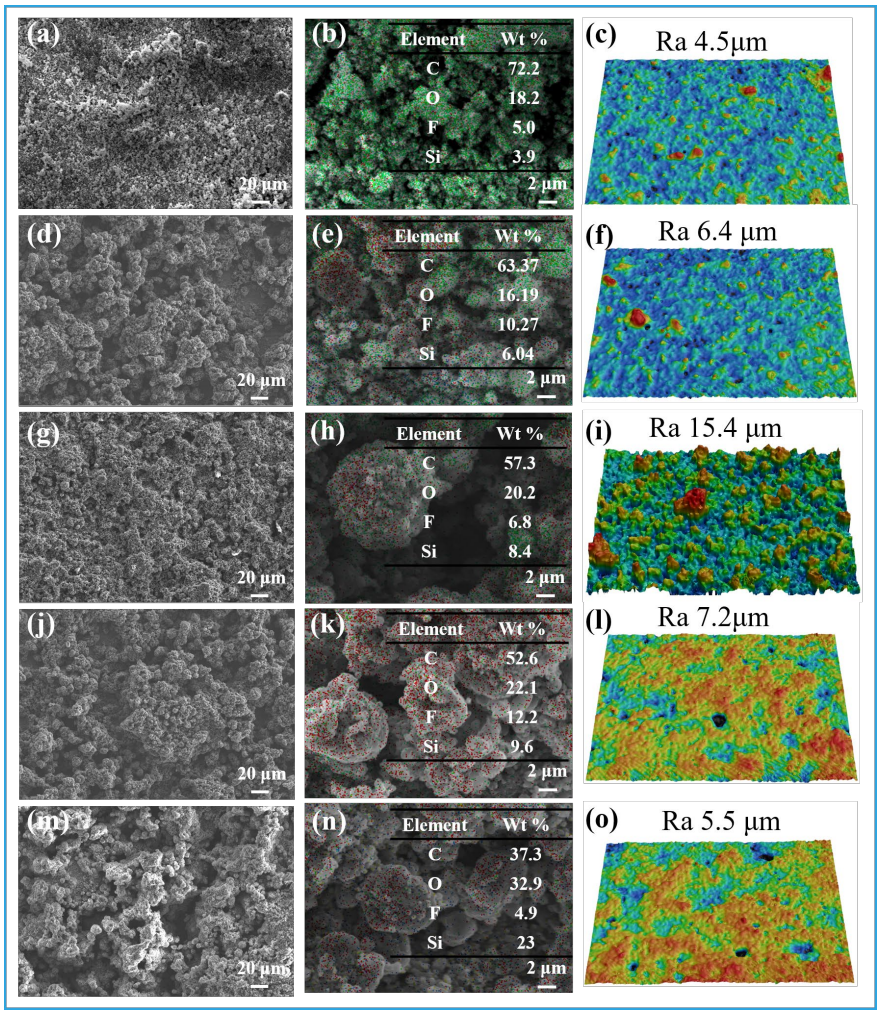

Fig 2. SEM image, corresponding EDS analysis and 3D structure diagram of different SiO2/HWCNTs mass ratios: (a-c) SHC0/4, (d-f) SHC1/3, (g-i) SHC1/1, (j-l) SHC3/1, (m-o) SHC4/0.

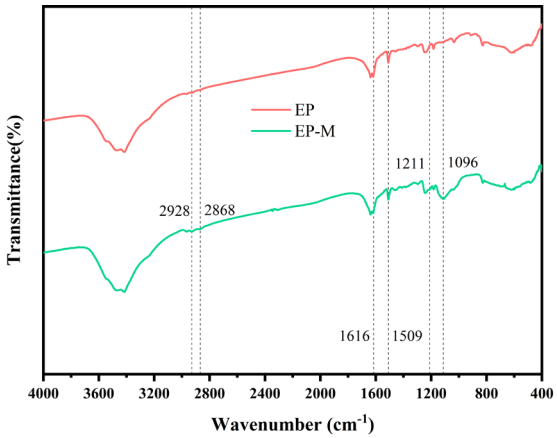

Fig 3. FTIR of epoxy resin and modified epoxy resin.

3.2. Wettability and photothermal conversion capability

As depicted in Fig. 4a, the wettability characteristics of various coatings were systematically investigated. The magnesium alloy substrate exhibited a water contact angle (WCA) of 37.3°, indicative of hydrophilicity, due to its smooth surface and high surface tension. In contrast, the EP-M coating achieved a WCA of 139°, demonstrating hydrophobicity through synergistic surface roughening and low surface energy modification. Notably, all HWCNTs/EP composite coatings exhibited superhydrophobicity with maximum WCA reaching 156.7°, representing approximately fourfold enhancement compared to the substrate. This remarkable performance confirms that the synergistic combination of modified epoxy resin and nanoparticles effectively engineered the coating's superhydrophobic properties. As evidenced in Fig. 4b-d, the photothermal performance of coatings demonstrates an initial enhancement followed by gradual reduction under light irradiation. The magnesium alloy substrate exhibited a temperature elevation to merely 33.8 °C within 200 s, whereas the EP-M coating achieved 41.2 °C, attributable to the lower specific heat capacity of epoxy resin that facilitates more pronounced temperature rise under equivalent heat absorption. Notably, SHC4/0 to SHC1/3 coatings displayed substantially enhanced photothermal conversion efficiency with maximum temperatures reaching 69 °C (35.2 °C higher than the substrate), achieved through the inherent black coloration of carbon nanotubes that significantly reduces visible light reflectivity. In contrast, SHC0/4 coating exhibited inferior performance with a maximum temperature of 27.3 °C, even lower than the substrate. All coatings exhibited prompt thermal dissipation to ambient following light source deactivation, demonstrating robust photothermal conversion capabilities. The results in Fig. 4e reveal that even after five cyclic irradiation-cooling tests, the SHC coatings exhibit negligible variation in their maximum equilibrium temperatures, demonstrating excellent thermal stability. This phenomenon can be attributed to the photothermal conversion

mechanism of carbon nanotubes, primarily involving lattice vibrations. Under solar irradiation, numerous loosely-bound electrons are excited from π to π* orbitals. These excited electrons dissipate the absorbed energy through phonon-phonon coupling while returning to ground states, simultaneously inducing lattice-scale vibrations that confer superior structural stability to the coatings[43-45].

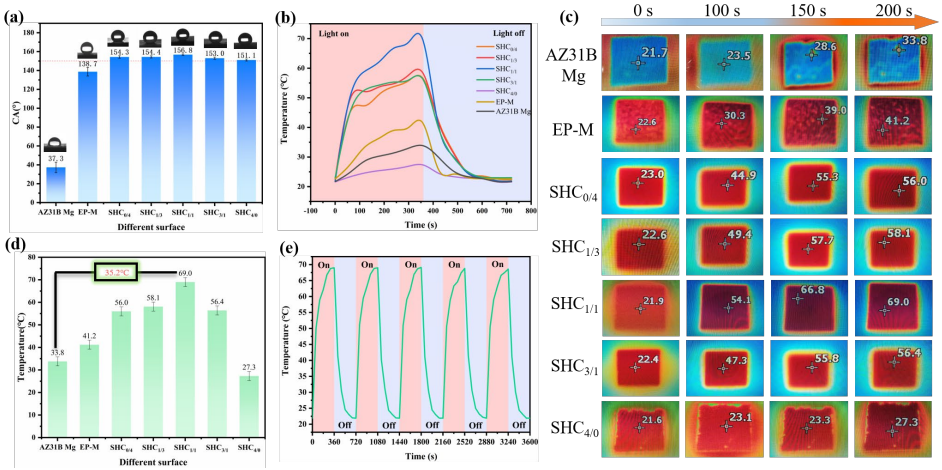

Fig 4. (a) CA of different coating surfaces, (b) photothermal temperature rise curves of coatings with different proportions, (c) comparison of maximum temperature of different coatings, (d) photothermal cycle curve under one sunlight intensity, (e) infrared thermogram of different surfaces.

3.3. Static delay icing performance

The anti-icing performance of HWCNTs/EP composite coatings was evaluated by monitoring droplet freezing behavior and freezing durations on different surfaces at -15 °C. As illustrated in Fig. 5a, sequential images of 10 μL droplets during freezing clearly demonstrate the ice-resistant properties of fabricated coatings through distinct droplet states at identical freezing stages. For the magnesium alloy substrate, the droplet rapidly turned opaque with a pronounced conical tip at 12 s, indicating complete freezing[46]. The EP-M hydrophobic surface marginally prolonged freezing time due to its moderate hydrophobicity, maintaining partial liquid state at 12 s with limited ice nucleation at the bottom, followed by full freezing at 50 s. The SHC4/0 superhydrophobic coating, benefiting from its high contact angle, retained liquid state until 608 s. Notably, the SHC0/4 superhydrophobic surface exhibited further extended freezing duration, attributed to synergistic effects between the black HWCNTs (enhancing photothermal conversion/heat absorption) and superhydrophobicity. Remarkably, the SHC1/1 coating, incorporating both EP and HWCNTs, achieved optimal performance: HWCNTs anchored on EP aggregated surfaces formed nano-mastoid structures, significantly amplifying surface roughness and creating intricate internal architectures. This design synergistically enhanced atmospheric heat absorption while preserving superhydrophobicity and photo-

thermal characteristics, ultimately delaying droplet freezing to 1026 s. Compared with the substrate, this represents a 1014 s extension in freezing time, demonstrating exceptional anti-icing performance.

The ice formation process can be fundamentally divided into two critical stages: nucleation and crystal growth[47]. The anti-icing mechanism of superhydrophobic surfaces primarily relies on effectively suppressing the droplet nucleation stage to delay freezing progression. The ice nucleation rate can be quantitatively evaluated using the following equation (1)[48, 49]:

$$R(T) = R_{\text{bulk}}(T)V + R_{\text{lg}}(T)S_{\text{lg}} + R_{\text{sl}} + R_{\text{sl}}(T)S_{\text{sl}} \quad (1)$$

Where: $R(T)$, $R_{\text{bulk}}(T)$, $R_{\text{lg}}(T)$ and $R_{\text{sl}}(T)$ represent the total nucleation rate, volume nucleation rate, liquid-gas and solid-liquid interface nucleation rate related to temperature respectively; V, Slg and Ssl are liquid volume, liquid-gas contact area and solid-liquid contact area respectively; T means the temperature. As shown in the equation, ice nucleation formation is closely associated with surface wettability, surface structure, and temperature. This achieves superhydrophobic anti-icing performance (Fig. 5b) through the fabrication of high-roughness micro-nano structures combined with hydrophobic modification. This approach effectively reduces both the contact area between the coating surface and ice nucleation sites (specifically decreasing the solid-liquid interfacial area) and the interfacial thermal conduction through these interfaces.

From the perspective of thermodynamics, the heat exchange between the environment and water droplets is mainly conducted through conduction and radiation, and the heat transfer equation is expressed as follows[50]:

$$\Delta Q = Q_{\text{s}} - Q_{\text{ls}} \quad (2)$$

Where ΔQ means the heat absorbed by the droplet per unit time, Qs means the heat obtained per unit time, and Qls is the heat lost at the solid-liquid interface per unit time. For the substrate, the heat gained from water droplets is significantly less than the thermal loss experienced at the cold interface, resulting in ΔQ<0. Over time, the cumulative heat loss from the droplet gradually increases. When the lost heat surpasses the gained heat, the droplet ultimately freezes completely. In contrast, the micro-nano structured photothermal superhydrophobic surface exhibits a Cassie-Baxter state, forming an air layer between the surface and the droplet. This configuration markedly reduces the solid-liquid contact area, thereby diminishing heat dissipation from the droplet to the cold surface and prolonging freezing time. The heat transfer equation can be expressed as[51, 52]:

$$\Delta Q = Q_{\text{s}} - Q_{\text{ls}} + Q_{\text{lg}} + Q_{\text{pt}} \quad (3)$$

Where Qlg means the heat loss at the gas-liquid interface per unit time, and Qpt is the heat generated by the surface photothermal effect per unit time. Additionally,

the highly spherical morphology of water droplets on superhydrophobic surfaces increases their contact area with air, thereby enhancing heat absorption capacity from ambient air through conduction or radiation processes (Fig. 5c). These combined factors collectively reduce the thermal dissipation per unit time of droplets, resulting in prolonged freezing delay time on superhydrophobic surfaces. As shown in Fig. 6, comparative analysis of icing initiation times across different surfaces demonstrates that the fabricated photothermal superhydrophobic coating significantly delays the freezing process on magnesium alloy surfaces. By minimizing solid-liquid contact area and reinforcing thermal barrier effects, this coating effectively suppresses ice crystal nucleation and growth, ultimately achieving exceptional anti-icing performance.

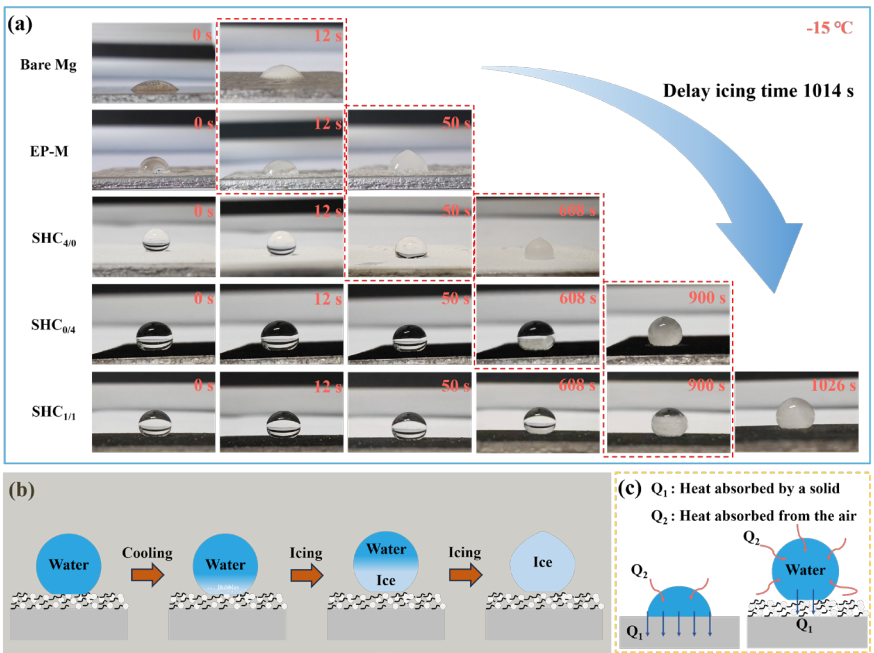

Fig 5. (a) Anti-icing performance of different surfaces, (b) static icing mechanism on superhydrophobic surfaces, (c) heat transfer model of hydrophilic and superhydrophobic surfaces.

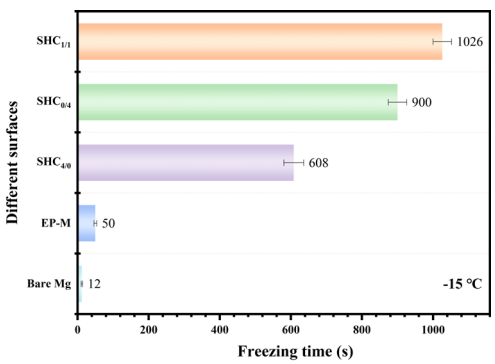

Fig 6. Icing time of different coatings.

3.4. Photothermal deicing performance

Although photothermal superhydrophobic coatings exhibit superior anti-icing performance compared to conventional superhydrophobic coatings, complete prevention of ice formation remains challenging under extreme low-temperature and high-humidity conditions. To validate the photothermal deicing efficacy of the fabricated coating in practical environments, a series of performance evaluation experiments were conducted. As illustrated in Fig. 7a, controlled 1 cm^3 water droplets were frozen into ice blocks at -15 °C and placed on magnesium alloy substrates, modified epoxy resin (EP-M) coatings, and SHC coating surfaces, respectively. The samples were irradiated using a xenon lamp simulating solar irradiation at 1 sun intensity. Results demonstrated that ice blocks on the magnesium alloy substrate required 421 s for complete melting under identical intensity. In contrast, melting time was substantially reduced to 146 s for ice blocks on the EP-M coating. However, the SHC4/0 superhydrophobic coating exhibited prolonged melting time of 397 s, representing only a 24 s reduction compared to the substrate. From the theoretical perspective of light absorption, incident photons interact with microscopic particles (ions, electrons, and atoms) within materials, inducing complex optical phenomena including transmission, scattering, absorption, and reflection. When surface roughness is significantly smaller than the incident light wavelength, scattering effects can be reasonably neglected compared to other optical mechanisms. Under such conditions, incident light energy distribution is predominantly governed by three fundamental mechanisms: transmission, absorption, and reflection. Accordingly, material light absorption efficiency can be calculated using equation (4)[13]:

$$A=1-R-T \quad (4)$$

Where: A is the absorption rate, R means the reflectivity, T is the transmissivity. The SHC0/4 superhydrophobic coating demonstrates exceptionally low reflectivity due to the intrinsic black coloration of HWCNTs, enabling high light absorption efficiency. Consequently, ice blocks on this coating surface completely melted within 56 s, followed by spontaneous ice shedding facilitated by its superhydrophobicity. Remarkably, the SHC1/1 composite coating incorporating both EP and HWCNTs achieved ice shedding within 44 s, representing nearly a ten-fold reduction in melting time compared to the magnesium alloy substrate. From the perspective of wetting theory, when heated, ice melts progressively from the bottom upward on superhydrophobic surfaces. During this process, the ice transitions from the Wenzel state to the Cassie-Baxter state, forming a thin interfacial water film that substantially reduces ice adhesion strength. This enables ice detachment under gravitational forces or mild natural wind (Fig. 7b). This mechanism effectively mitigates structural damage to micro-nano hierarchical textures during repeated icing/deicing cy-

cles, thereby enhancing the coating's operational longevity.

Furthermore, the photothermal deicing mechanism of this multi-structured superhydrophobic composite surface can be elucidated through Fig. 7c, where the thermal content of a droplet is denoted as Q1, and the heat generated by the coating under irradiation is designated as Q2. Under low-temperature, light-free conditions, droplets adhere to the coating surface and resist removal. During this phase, the droplet's thermal energy (Q1) rapidly dissipates into the surrounding cold medium, leading to droplet freezing. However, when exposed to intensity, the intricate micro-nano hierarchical structures formed by EP and HWCNTs on the photothermal superhydrophobic surface create "optical traps" that efficiently absorb incident light while minimizing reflection. Concurrently, HWCNTs are stimulated to generate substantial heat (Q2), which transfers through the coating surface to the frozen droplet, enabling active deicing and achieving high-efficiency photothermal ice removal. Notably, the magnitude of Q2 generation critically depends on the material's light absorption capability. The reflectivity of the light-absorbing layer toward incident radiation can be calculated using equation (5)[53]:

$$R = \left| \frac{Z(\omega) - Z_0(\omega)}{Z(\omega) + Z_0(\omega)} \right|^2 \tag{5}$$

Where: Z(ω) is the impedance of the material absorption layer; Z0(ω) means the impedance of free space, which meets the following relationship:

$$Z(\omega) = \sqrt{\mu(\omega)\mu_0 / \varepsilon(\omega)\varepsilon_0} \tag{6}$$

$$Z_0(\omega) = \sqrt{\mu_0 / \varepsilon_0} \tag{7}$$

In the provided equations, ε(ω) and μ(ω) represent the complex permittivity and complex permeability of the material, respectively, while ε0 and μ0 denote the permittivity and permeability of free space. When μ(ω) equals ε(ω), the material satisfies the impedance matching condition Z(ω)=Z0(ω), achieving minimal reflectivity and maximum light absorption efficiency. Furthermore, the electromagnetic properties governing light absorption at the surface can be characterized by the effective complex permittivity ε(ω)eff and effective complex permeability μ(ω)eff. According to Maxwell-Garnett theory[54], the ε(ω)eff of the composite surface depends on the permittivity of its constituent materials ε(ω) and the dielectric constant of air εair, which can be calculated using equation (8)[53]:

$$\frac{\varepsilon(\omega)_{eff} - \varepsilon_{air}}{\varepsilon(\omega)_{eff} + 2\varepsilon_{air}} = (1 - V_{\text{air}}) \times \frac{\varepsilon(\omega) - \varepsilon_{air}}{\varepsilon(\omega) + 2\varepsilon_{air}} \tag{8}$$

Where: V_{air} represents the volume fraction of air within the material. Therefore, enhancing the structural roughness of the superhydrophobic surface significantly increases air entrapment at the material interface, thereby reducing surface reflectivity and improving the light absorption performance of the photothermal superhydrophobic surface. As shown in Fig. 8, comparative ice-melting durations across different surfaces reveal that the fabricated photothermal superhydrophobic coating significantly reduces the ice-melting duration on magnesium alloy substrates, demonstrating exceptional photothermal deicing efficacy. These synergistic effects collectively enhance the thermal energy absorption per unit time of the coating, thereby accelerating ice-melting on superhydrophobic surfaces. Specifically, the optimized superhydrophobic coating exhibits superior solar energy capture and conversion into thermal energy, a critical factor for rapid ice removal. Additionally, enhanced light absorption minimizes thermal dissipation from the coating surface under intensity, further improving deicing efficiency.

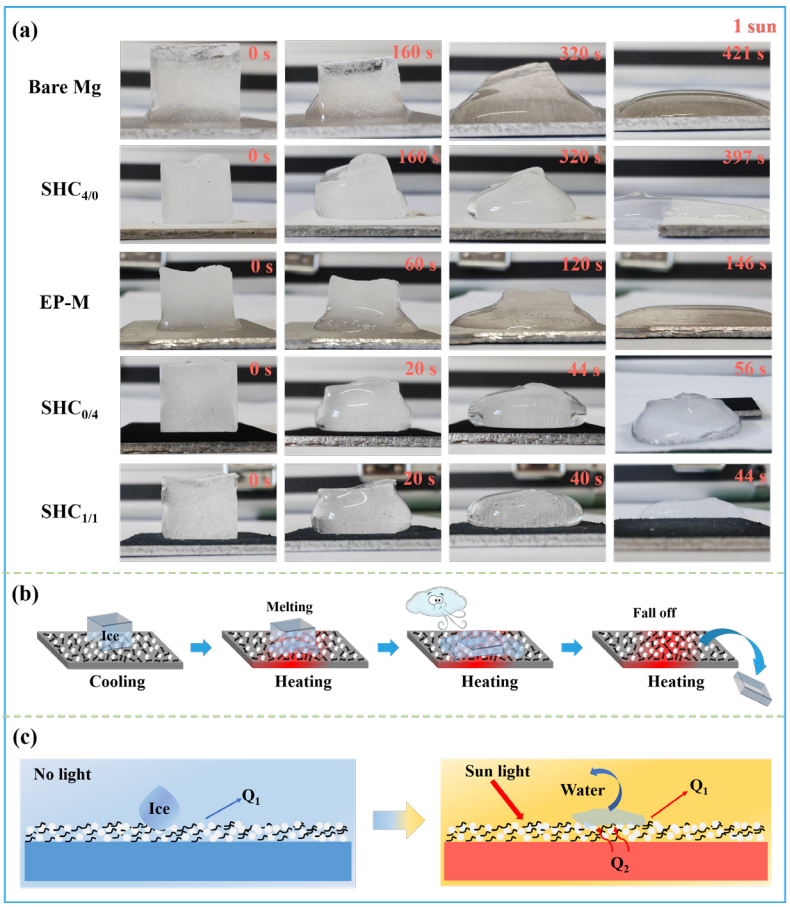

Fig 7. (a) Photothermal deicing performance of different surfaces, (b) ice melting mechanism on superhydrophobic surfaces, (c) light absorption mechanism of composite superhydrophobic surfaces.

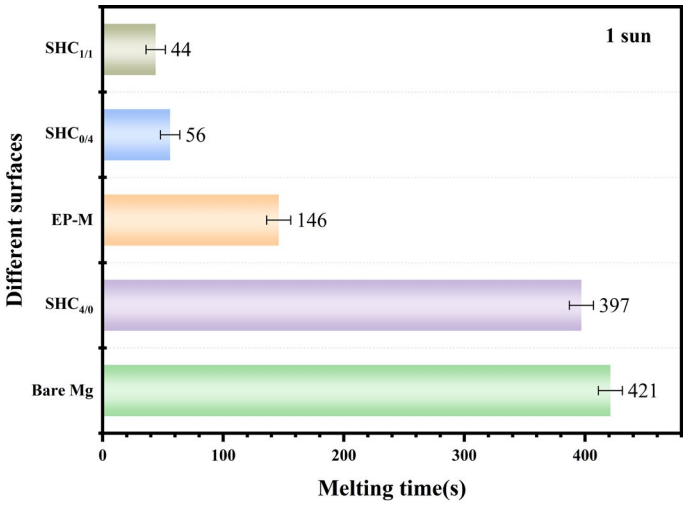

Fig 8. Ice melting time of different coatings.

3.5. Self-cleaning and anti-fouling properties

The inevitable accumulation of solid contaminants on material surfaces in practical applications not only obstructs sunlight but also adversely affects photothermal efficiency. In this study, comparative self-cleaning tests were conducted on magnesium alloy substrates and HWCNTs/EP composite coating surfaces using sand particles as model contaminants. As demonstrated in Fig. 9a, substantial residual water and contaminants remained on bare substrates after water droplet application, while the HWCNTs/EP composite coating achieved complete contaminant removal through rolling droplets, exhibiting lotus leaf-like self-cleaning behavior. This phenomenon originates from the ultralow solid-liquid contact area and surface energy of the superhydrophobic surface, enabling rapid droplet shedding with contaminant entrainment. Meanwhile, the coating demonstrated exceptional liquid repellency against four common pollutants (tea, cola, milk, coffee), maintaining superhydrophobicity as shown in Fig. 9b. anti-fouling tests (soak for 30 seconds) revealed no liquid residue on HWCNTs/EP composite coating surfaces compared to contaminated substrates (Fig. 9c). The superior self-cleaning and anti-fouling performance stems from two fundamental characteristics: 1) hierarchical micro-nano structures enhancing surface roughness to achieve Cassie-Baxter state; 2) ultra-low surface energy minimizing liquid spreading and adhesion through thermodynamic stabilization. These combined attributes significantly improve photothermal conversion efficiency and operational durability in real-world applications.

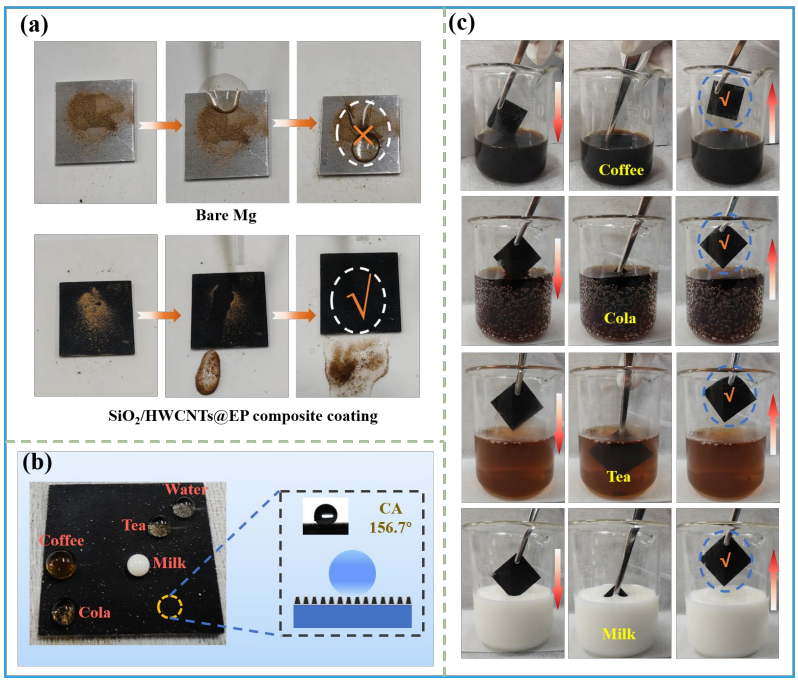

Fig 9. (a) Self-cleaning test, (b) photos of different liquid pollutants on the SiO2/HWCNTs@EP coating, (c) anti-fouling performance test.

4. Conclusions

In summary, this work fabricated a HWCNTs/EP composite coating with photothermal superhydrophobic performance via a "one-step spraying" method. This involved spraying a mixed solution of modified epoxy resin and HWCNTs onto AZ31B magnesium alloy substrates. The coating exhibits exceptional photothermal conversion capability and effective anti-icing/deicing performance while maintaining superior self-cleaning properties. Notably, the coating extends water droplet freezing time to 1026 s at -15°C. Under 1-sun intensity, the surface temperature reaches 69 °C within 360 s and achieves complete deicing in 44 s, effectively preventing ice formation in low-temperature environments. Furthermore, surface contaminants exhibit significantly reduced adhesion strength and are readily removed by water flushing. This work provides novel perspectives for scalable deployment of photothermal superhydrophobic coatings in anti-icing/deicing applications.

References

[1] C.L. Guo, K. Liu, C.C. Ma, P. Sun, L. Liang. Constructing a hierarchical coating with photothermal superhydrophobic property by spraying and modification on polyurethane foam for anti-icing and deicing, Appl. Therm. Eng. 236 (2024) 121907.

[2] H. Ducloux, B.E.K. Nygaard. Ice loads on overhead lines due to freezing radia-tion fog events in plains, Cold Reg. Sci. Tech. 153 (2018) 120-129.

[3] H. Su, J. Yang. Design and preparation of multiple silica particles and study on superhydrophobic modified epoxy resin, J. Polym. Res. 30 (6) (2023) 238

[4] Y.H. Cao, W.Y. Tan, Z.L. Wu. Aircraft icing: An ongoing threat to aviation safety, Aerosp.

Sci. Technol. 75 (2018) 353-385.

[5] L. Makkonen. Ice Adhesion - Theory, Measurements and Countermeasures, J. Adhes. Sci. Technol. 26 (4-5) (2012) 413-45.

[6] T.X. Yu, L.F. Qiao, X. Liu. Cable deicing device based on ice melting and me-chanical ice breaking, Journal of Physics: Conference Series, 1865 (3) (2021) 032074.

[7] Z.C. Zhang, A. Lusi, H.Y. Hu, X.L. Bai, H. Hu. An experimental study on the det-rimental effects of deicing fluids on the performance of icephobic coatings for aircraft icing mitigation, Aerosp. Sci. Technol.119 (2021) 107090.

[8] C.B. Chang, I. Noh, N. Zhou, J. Jeon, Y.B. Wang, H.D. Kim, Q.Q. Liu, H. Ohkita, X.L. Tao, B.B. Wang. Construction of robust superhydrophobic surfaces with electrothermal, photothermal properties using simple spraying method, Surf. Interfaces. 52 (2024) 104879.

[9] W. Huang, J.X. Huang, Z.G. Guo, W.M. Liu. Icephobic/anti-icing properties of superhydrophobic surfaces, Adv. Colloid Interface Sci. 304 (2022) 102658.

[10] X.K. Wang, J. Zeng, J. Li, X.Q. Yu, Z.K. Wang, Y.F. Zhang. Beetle and cac-tus-inspired surface endows continuous and directional droplet jumping for efficient water harvesting, J. Mater. Chem. A. 9 (3) (2021) 1507-16.

[11] H.Y. Xiang, Y. Yuan, X. Dai, T. Zhu, Y.Y. Zhao, L.B. Song, R.J. Liao. A novel su-perhydrophobic Al conductor with excellent anti-icing performance and its mechanism, Surf. Interfaces. 46 (2024) 104138.

[12] Z.J. Chen, B.B. Shen, Y.L. Zhang, H.L. Guo, Z. Chen, R. Wei, J. Hu. Superhydro-phobic coating of a modified calcium sulfate whiskers@SiO2-F/TPU for an-ti-icing applications, Adv. Powder Technol. 35 (3) (2024) 104362.

[13] Z.H. Zhao, H.W. Chen, Y.T. Zhu, X.L. Liu, Z.L.L. Wang, J.C. Chen. A robust su-perhydrophobic anti-icing/deicing composite coating with electrothermal and auxiliary photothermal performances, Compos. Sci. Technol. 227 (2022) 109578.

[14] J.M. Wan, J. Xu, S.Y. Zhu, B. Wang, J. Li, G.D. Ying, K.F. Chen. Flexible biomi-metic materials with excellent photothermal performance and superhydro-phobicity, J. Colloid Interface Sci. 629 (2023) 581-90.

[15] Y.B. Liu, Y. Wu, Y.Z. Liu, R.N. Xu, S.J. Liu, F Zhou. Robust Photothermal Coating Strategy for Efficient Ice Removal, ACS Appl. Mater. Interfaces. 12 (41) (2020) 46981-90.

[16] W. Sun, Y.T. Wei, Y.H. Feng, F.Q. Chu. Anti-icing and deicing characteristics of photothermal superhydrophobic surfaces based on metal nanoparticles and carbon nanotube materials, Energy. 286 (2024) 129656.

[17] L.S. Wu, P. Liu, X.C. Hua, Z.G. Guo, W.M. Liu. Photothermal superhydrophobic membrane based on breath figure: Anti-icing and deicing, Chem. Eng. J. 480 (2024) 147553.

[18] Y. Li, W. Ma, Y.S. Kwon, W.H. Li, S.H. Yao, B.L. Huang. Solar Deicing Nano-coatings Adaptive to Overhead Power Lines, Adv. Funct. Mater. 32 (25) (2022) 2113297.

[19] R. Zhang, Z.M. Ding, K.Q. Wang, H.L. Zhang, J.J. Li. Enhanced Anti/Deicing Performance on Rough Surfaces Based on The Synergistic Effect of Fluorinat-ed Resin and Embedded Graphene, Small methods, 8 (7) (2024) e2301262.

[20] Y.H. Zhang, X.Q. Fan, W.X. Zhu, X.R. Li, M. Cai, Y. Huang, C. He, L. Zhang, B. Lin, M.H. Zhu. Probing photothermal superhydrophobic behaviors of gra-phene&SiO2 hybrid coating for anti-freeze application, Ceram. Int. 49 (20) (2023) 33020-8.

[21] Y.H. Cheng, Y.R. Wang, X. Zhang, J.M. Zhang, Z.Y. He, J.J. Wang, J. Zhang. Spon-taneous, scalable, and self-similar superhydrophobic coatings for all-weather deicing, Nano Res. 16 (5) (2023) 7171-9.

[22] X.D. Liu, S.Z. Li, Y.L. Wu, T.F. Guo, J.H. Xie, J.Q. Tao, L. Dong, Q.P. Ran. Robust All-Waterborne Superhydrophobic Coating with Photothermal Deicing and Passive Anti-icing Properties, ACS Appl. Mater. Interfaces. 15 (37) (2023) 44305-44313.

[23] Z.H. Zhao, Q. Zhang, X.D. Song, J. Chen, Y.T. Ding, H. Wu, S.Y. Guo. Versatile Melanin-Like Coatings with Hierarchical Structure toward Personal Thermal Management, Anti-Icing/Deicing, and UV Protection, ACS Appl. Mater. Inter-faces. 15 (2023) 3522-3533.

[24] Y.H. Yang, Y.Y. Tu, Z.Y. Lou, X.F. Gui, J.L. Kong, Z.Z. Huang. Rapid UV-curable preparation of durable soybean oil-based superhydrophobic anti-icing surfac-es with excellent photothermal deicing property, Appl. Surf. Sci. 653 (2024) 159423.

[25] S. El Bakali, H. Ouadi, S. Gheouany. Wind turbine and PV power prediction using a deterministic data-driven model with variational mode decomposi-tion preprocessing, Trans. Inst. Meas. Control. 47 (7) (2025) 1413-28.

[26] M.V. Cardoso, A.C.P. Sant'Ana, M.S.R. Zangrando, C.A. Damante. Effects of photobiostimulation and antimicrobial photodynamic therapy associated with gingival grafts for root coverage: three-arm randomized clinical trial, Lasers Med. Sci. 40 (1) (2025) 190.

[27] C.J. Kho, S. Moon, J.Y. Lee. Secondary Organic Aerosol Formation through Photochemical Oxidation of NO and SO2 in an Indoor Smog Chamber, J. Envi-ron. Eng.-ASCE. 151 (6) (2025) 04025027.

[28] H.B. Yuan, L. Wei, J.P. Wang, M.M. Zhao, G.Q. Chen, T.L. Xing, Z. Chen. Robust and breathable electronic textiles with anti-icing and photothermal deicing properties modified by ZIF-8/polypyrrole, Chem. Eng. J. 509 (2025) 161569.

[29] Y.L. Wu, L. Dong, X. Shu, Y. Yang, P. Feng, Q.P. Ran. Recent advancements in photothermal anti-icing/deicing materials. Chem. Eng. J. 469 (2023) 143924.

[30] W. Tong, M.M. Han, C. Ma, Z. Wu, N. Wang, N. Du, T.F. Xiang, J.S. Zhu. Em-powering Photovoltaic Panel Anti-Icing: Superhydrophobic Organic Compo-site Coating with In Situ Photothermal and Transparency, ACS Appl. Mater. Interfaces. 16 (24) (2024) 31567-75.

[31] T.F. Xiang, X.X. Chen, Z. Lv, W. Tong, J. Cao, Y.Z. Shen, B.K. Liao, Y.N. Xie, S.H. Zhang. Stable photothermal solid slippery surface with enhanced anti-icing and de-icing properties, Appl. Surf. Sci. 624 (2023) 157178.

[32] Y. Yuan, C.Z. Zhang, B.C. Jiang, Y.H. Lei, Z.T. Li, K. Sun, Y.L. Zhang. A robust photothermal superhydrophobic anti/deicing composite coating fabricated from BP/SiO2 on a modified fluorocarbon coating base, Prog. Org. Coat. 196 (2024) 108725.

[33] Y.J. Gou, J. Han, Y.D. Li, Y. Qin, Q.G. Li, X.H. Zhong. Research on Anti-Icing Performance of Graphene Photothermal Superhydrophobic Surface for Wind Turbine Blades, Energies. 16(1) (2022) 408.

[34] X.Y. Li, H.Q. Su, H. Li, X. Tan, X. Lin, Y.H. Wu, X.L. Xiong, Z.G. Li, L.H. Jiang, T. Xiao, W.F. Chen, X.Y. Tan. Photothermal superhydrophobic surface with good corrosion resistance, anti-/deicing property and mechanical robustness fab-ricated via multiple-pulse laser ablation, Appl. Surf. Sci. 646 (2024) 158944.

[35] X.H. Liu, H.M. Liu, Y. Li, F. Teng, C. Liang. Superhydrophobic surface of hybrid nanocomposites made of TiO2 and multi-walled carbon nanotubes: Photo-thermal ice removal performance and wear resistance, Appl. Surf. Sci. 640 (2023) 158318.

[36] L. Zhang, C.L. Gao, L.S. Zhong, L.M. Zhu, H. Chen, Y.P. Hou, Y.M. Zheng. Robust photothermal superhydrophobic coatings with dual-size micro/nano struc-ture enhance anti-/deicing and chemical resistance properties, Chem. Eng. J. 446 (2022) 137461.

[37] B.R. Wu, X. Cui, H.Y. Jiang, N. Wu, C.Y. Peng, Z.F. Hu, X.B. Liang, Y.G. Yan, J. Huang, D.S. Li. A superhydrophobic coating harvesting mechanical robustness, passive anti-icing and active deicing performances, J. Colloid Interface Sci. 590 (2021) 301-10.

[38] X. Xiao, X.P. Wei, J. Wei, J. Wang. Multifunctional Fe3O4-based photothermal superhydrophobic composite coating for efficient anti-icing/deicing, Sol. En-ergy Mater. Sol. Cells. 256 (2023) 112313.

[39] X. Yi, X. Wei, K. Shefiu, C.X. Qiu, Y.F. Hu, lP. Parkin , S.W. Wang, H.Y. Wang, J.W. Chen, L. Li, Z. Chen, H.J. Sun, X.J. Zhao. Robust superamphiphobic coatings with gradient and hierarchical architecture and excellent anti-flashover per-formances, Nano Res. 15(8) (2022) 7565-76.

[40] H. Xie, J.F. Wei, S.Y. Duan, Q. Zhu, Y.F. Yang, K. Chen, J.J. Zhang, L.X. Li, J.P. Zhang. Non-fluorinated and durable photothermal superhydrophobic coatings based on attapulgite nanorods for efficient anti-icing and deicing, Chem. Eng. J. 428 (2022) 132585.

[41] X. Liu, T.C. Zhang, Y.X. Zhang, J.S. Rao, S.J. Yuan. A route for large-scale prepa-ration of

multifunctional superhydrophobic coating with electrochemical-ly-modified kaolin for efficient corrosion protection of magnesium alloys, J. Magnes. Alloy. 10 (11) (2022) 3082-99.

[42] Y.H. Lei, G.J. Ye, B.C. Jiang, L. Wen., X.C. Mo, X.J. Lei, Y.L. Zhang, Y. Yuan, X.T. Chang. Ice-resistant Fe3O4@PPy coating: Enhancing stability and durability with photothermal super hydrophobicity, Prog. Org. Coat. 196 (2024) 108704.

[43] Y.L. Wu, L. Dong, X. Shu, Y. Yang, P. Feng, Q.P. Ran. Recent advancements in photothermal anti-icing/deicing materials, Chem. Eng. J. 469 (2023) 143924.

[44] C. Zhang, H.Q. Liang, Z.K. Xu, Z.K. Wang. Harnessing Solar‐Driven Photo-thermal Effect toward the Water–Energy Nexus, Adv. Sci. 6 (18) (2019) 1900883.

[45] C.j. Chen, Y.D. Kuang, L.B. Hu. Challenges and Opportunities for Solar Evapo-ration, Joule. 3 (3) (2019) 683-718.

[46] Y. Guo, H.B. Zhao, C.S. Zhang, G.Q. Zhao. Super photothermal/electrothermal response and anti-icing/deicing capability of superhydrophobic multi-walled carbon nanotubes/epoxy coating, Chem. Eng. J. 497 (2024) 154383.

[47] A. Alizadeh, M. Yamada, R. Li, W. Shang, S. Otta, S. Zhong, L.H. Ge, A. Dhi-nojwala, K.R. Conway, V. Bahadur, A.J. Vinciquerra, B. Stephens, M.L. Blohm. Dynamics of ice nucleation on water repellent surfaces, Langmuir. 28 (6) (2012) 3180-6.

[48] Q.T. Fu, E.J. Liu, P. Wilson, Z. Chen. Ice nucleation behaviour on sol-gel coat-ings with different surface energy and roughness, Phys. Chem. Chem. Phys. 17 (33) (2015) 21492-500.

[49] S. Jung, M. Dorrestijn, D. Raps, A. Das, C.M. Megaridis, D. Poulikakos. Are Su-perhydrophobic Surfaces Best for Icephobicity?, Langmuir, 27 (6) (2011) 3059-66.

[50] H. He, W. Huang, Z.G. Guo. Superhydrophobic and photothermal SiC/TiN du-rable composite coatings for passive anti-icing/active deicing and de-frosting, Mater. Today Phys. 30 (2023) 100927.

[51] Z.T. Xie, H. Wang, Y. Geng, M. Li, Q.Y. Deng, Y. Tian, R. Chen, X. Zhu, Q. Liao. Carbon-Based Photothermal Superhydrophobic Materials with Hierarchical Structure Enhances the Anti-Icing and Photothermal Deicing Properties, ACS Appl. Mater. Interfaces. 13 (40) (2021) 48308-48321.

[52] Y. Liu, X.L. Li, J.F. Jin, J.A. Liu, Y.Y. Yan, Z.W. Han, L.Q. Ren. Anti-icing proper-ty of bio-inspired micro-structure superhydrophobic surfaces and heat trans-fer model, Appl. Surf. Sci. 400 (2017) 498-505.

[53] M. Agarwal, M.K. Meshram. Metamaterial-based dual-band microwave ab-sorber with polarization insensitive and wide-angle performance, AIP Adv. 8 (9) (2018) 095016.

[54] V.A. Markel. Introduction to the Maxwell Garnett approximation: tutorial, J. Opt. Soc. Am. A-Opt. Image Sci. Vis. 33 (7) (2016) 1244-1256.